ASSESSMENT OF BUILDINGS AND ELECTRICAL FACILITIES DAMAGED BY FLOOD AND EARTHQUAKE FROM SATELLITE IMAGERY

Yi Ma[a], Fangrong Zhou[a], Gang Wen[a], Hao Gen[a], Ran Huang[a], Guoqing Liu[b,*], Ling Pei[b]

[a]Electric Power Research Institute, Yunnan Power Grid Company ltd., Kunming, China - 42971995@qq.com, 42783590@qq.com, 1192381484@qq.com, whugenghao@163.com, 50276157@qq.com
[b]School of Electronic Information and Electrical Engineering, Shanghai Jiao Tong University, Shanghai, China - (guoqing_liu, ling.pei)@sjtu.edu.cn

Commission III, WG III/1

KEY WORDS: Damage Assessment, Natural Disasters, Satellite Imagery, Buildings and Electrical Facilities, xBD Dataset, Building Localization.

ABSTRACT:

Natural disasters cause considerable losses to people's lives and property. Satellite images can provide crucial information of the affected areas for the first time, conducive to relieving the people in disaster and reducing the economic loss. However, the traditional satellite image analysis method based on manual processing drains workforce and material resources, which slowed the government's response to the disaster. Aiming at the natural disasters like floods and earthquakes that often happen in the south of China, we propose a dual-stage damage assessment method based on LEDNet and ResNet. Our method detects the changes between the satellite images captured before and after a disaster of the same area, segments the buildings, and evaluates the damage level of affected buildings. In addition, we calculate influence maps based on the damage scale to the building and estimate the damage situation for electrical facilities. We used images related to earthquakes and floods in the xBD dataset to train the network model. Moreover, qualitative and quantitative evaluations demonstrated that our method has higher accuracy than the xBD baseline.

1. INTRODUCTION

Natural disasters have brought significant losses to human society. Haiti earthquake caused 8 to 14 billion dollars loss, and more than 3 million people have been affected (Margesson and Taft-Morales, 2010). From June 2020, nearly 40 million people were displaced by the flood in the Yangtze River's upper and middle basins (Zhang and Xia, 2022). The frequency of sudden natural disasters increases due to climate change and global greenhouse gas emissions. Extreme storms hit Zhengzhou on 20 July 2021 with average precipitation 457.5mm (Cai et al., 2021).

After sudden natural disasters occur, accurate information and timely response are crucial to saving lives and reducing economic losses. It is slow to acquire affected area situations by capturing images on the ground. At worst, it may be impossible to take pictures from the ground like (Xiong et al., 2021) because of the environmental conditions after the disaster. Whereas satellite imagery can remote sense the affected area on a larger scale to grasp disaster information first. Through signal processing technologies such as image inpainting and super-resolution similar to (Wen et al., 2017), detailed information about the disaster area can be obtained in satellite images. We noticed that the traditional way of manual processing and analysis of satellite images by experts is time-consuming and laborious. This method tends to delay the disaster relief work, especially in flood, earthquake, and other large-scale disaster scenarios. Rapid and accurate automatic analysis methods are urgently needed to solve this problem.

In recent years, learning-based computer vision technology represented by the convolutional neural network(CNN) has made remarkable progress in image processing. Object detection network YOLO (Bochkovskiy et al., 2020) can detect and locate objects in the image. Semantic segmentation network SegNet (Badrinarayanan et al., 2017) can determine the object class of each pixel in the image. Instance segmentation network Mask-RCNN (He et al., 2017) can further segment the pixel mask of the object area in the image. These essential works provide the possibility to achieve the classification and segmentation on satellite images, such as detection of vehicles and other objects (Van Etten, 2018), analysis of flood area (Rahnemoonfar et al., 2020), extraction of fire boundary (Doshi et al., 2019), assessment of damaged buildings (Cooner et al., 2016).

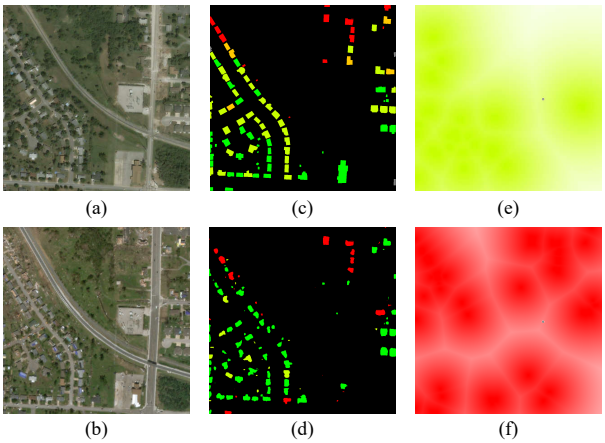

Figure 1. Results of our method.

We proposed a new method to assess the damage of buildings

* Corresponding author

and power facilities by using multi-temporary satellite images. At first, a two-stage procedure was used to evaluate damaged buildings. Similar to xBD baseline (Gupta et al., 2019), semantic segmentation was performed in the first stage to obtain the building mask. The second stage assessed the damage level of the buildings within the mask. LEDNet (Wang et al., 2019) was used to replace the U-Net (Ronneberger et al., 2015) of semantic segmentation in xBD baseline (Gupta et al., 2019). This pipeline was trained on xBD dataset (Gupta et al., 2019) by using the pre-disaster images and post-disaster images. The results of our experiment show that the average time of building damage assessment was decreased with better accuracy. The information of electrical facilities is also vital for disaster relief work, but there is no label about power utilities in the xBD dataset. Considering this, we computed influence maps to estimate the damage level of electrical facilities based on the damaged level of nearby buildings.

Figure 1 shows the results of our method. Figure 1 (a) and Figure 1 (b) are the pre-disaster and post-disaster satellite images from the xBD dataset. Figure 1 (c) is the ground truth of building damage level, where Figure 1 (d) is the building damage assessment result of our method. Different colors of the pixels indicate different levels of building damage: green represents “no-damage”, yellow-green represents “minor-damage”, orange represents “major-damage”, and red represents “destroyed”. Gray pixels in (c) indicate that the damage level cannot be determined (see Section 4.1 and Table 1). Figure 1 (e) and Figure 1 (f) are the influence maps of two damage levels, “minor-damage” and “destroyed”, and the circles in the image are the locations of power facilities. Based on the above influence maps we can estimate the scale of damage to electrical equipment based on the level of damage to the building. See Section 3.4 for details.

The main contributions of this paper are summarized as three points:

- We replaced U-Net in the xBD baseline model with LEDNet, achieved a more accurate and time-efficient assessment of damaged buildings.
- Based on the assessment of neighboring damaged buildings, we computed influence maps to evaluate the damage level of electrical facilities.
- By analyzing the evaluation results on the xBD dataset, we explained the strengths and weaknesses of damage assessment methods for buildings and electrical facilities and put forward the direction of improvement.

The organization of the rest of the paper is as follows. Section 2 reviews related works on change detection and assessment of buildings damaged on satellite imagery. We present our new method for damaged buildings and electrical facilities assessing in Section 3 . Section 4 describes the performance of this method on the testing set in the xBD dataset. Finally, we draw conclusions in Section 5.

2. RELATED WORK

The damage assessment’s primary purpose is to segment the building mask out and classify the damage level, such as no-damage, major-damage, and destroyed. Due to the lack of appropriate labeling in available datasets, most early research simplified the multi-classification task of building damage assessment to the change detection task of binary classification. These methods can determine whether a building is damaged but cannot get a damage level. This section introduces related research work from two aspects of change detection and building damage assessment.

2.1 Change detection of satellite imagery

The change detection task of satellite images was used to judge whether the ground surface features like forest have changed over a while. For example, Qi Zhixin et al. combine change vector analysis and support vector machines to detect land cover changes using polarimetric synthetic aperture radar (PolSAR) images (Qi et al., 2015). Inspired by the theory of meta-learning, Liu Hongying et al. improved the convolutional neural network and combined it with a graph neural network to achieve change detection in synthetic aperture radar and multispectral images (Liu et al., 2019). In order to explore the role that deep learning play in building damage detection, Francesco Nex et al. tested and evaluated the structural damage of buildings by using a convolutional neural network based on unmanned aerial vehicle (UAV) captured images (Nex et al., 2019). In terms of pure visible light satellite images, Maria Papadomanolaki et al. combined the fully convolutional neural network similar to U-Net (Ronneberger et al., 2015) structure and the long-short time modeling neural network of LSTM to present a new deep learning algorithm for the detection of urban environmental changes based on satellite imagery (Papadomanolaki et al., 2019).

If we have such prior that natural disasters cause changes in the ground surface, the damaged buildings will seem like changed between pre-disaster and post-disaster satellite images. From this point of view, FooldNet (Rahnemoonfar et al., 2020) determined whether buildings in flooded areas were affected can further help judge whether buildings are damaged. Ken Sakurada et al. was inspired by the change detection method and used CNN to determine whether buildings were washed away after the tsunami (Fujita et al., 2017). These change detection-based methods can usually only give a binary label of the damage to the building: the building is damaged (i.e., changed), or the building is not damaged (i.e., not changed), which are helpful for post-disaster analysis and assessment. However, considering the shortage of personnel and materials after the disaster, the more detailed information of building damage level we get, the more reasonable allocation of disaster relief resources can be executed. Although relevant work, has conducted multi-category change detection, such as Lu Hui et al. from Tsinghua University, more attention is paid to cultivated land area change, water area change, and urban area change (Lyu et al., 2016). The specific task of building damage rating assessment has attracted the researchers’ interest.

2.2 Assessment of damaged buildings

Different from most change detection works, building damage assessment can be divided into two sub-tasks. One task is building segmentation or building localization, that is, to determine the number and location of buildings in satellite images, which can be regarded as an image segmentation task. The other is detection or classification of building damage level, that is, to determine whether the building is no-damaged, minor-damaged, or major-damaged on the building mask, which can be regarded as an image classification task. Therefore the xBD baseline (Gupta et al., 2019) uses two networks for the building damage assessment. One segments the building area based on U-Net, and another classifies the damage level of each building.

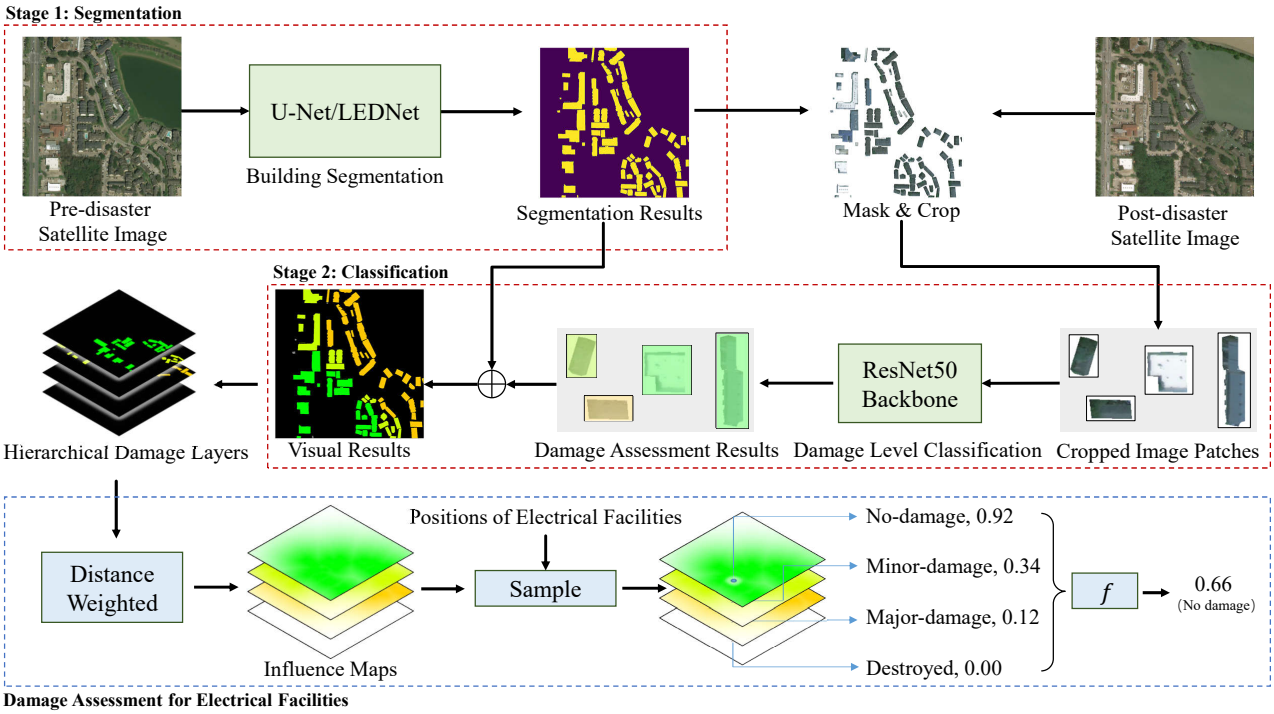

Figure 2. Pipeline of our method.

Chen et al. also used a two-stage method (Chen, 2021), which linked the RGB channels of pre-disaster and post-disaster images together. Then they studied the distribution characteristics of categories in the dataset and tested different loss functions to evaluate the effect for the network model. Finally, an interpretable heat map was given to show which parts of buildings have the most critical impact on damage classification. Liu Lanfa et al. noticed that the number of damaged buildings was not equal to the number of no damaged buildings, then introduced the categorical sample balance strategy in dataset processing (Ji et al., 2018). In the end, they compared the situation of building damage in the Haiti earthquake with a variety of different convolutional neural network models and assessed building damage based on CNN.

In theory, building damage assessment only needs to use post-disaster images. However, inspired by the change detection methods and the purpose of improving accuracy, the existing studies mostly use a pair of pre-disaster and post-disaster images to carry out the damage assessment of buildings. We call that "multi-temporal". Jihyeon Lee et al. proposed using multi-temporal images for building damage detection (Xu et al., 2019). Since there are some commonalities in feature extraction of multi-temporal images, the siamese network is suitable for building damage assessment. Hanxiang Hao et al. explored the utilization of multi-temporal images (Hao et al., 2020). After experiments such as channel cascade and multi-temporal image difference, siamese network and attention mechanism were introduced to improve the detection accuracy. Rodrigo Caye Daudt et al. explored three fully convolutional neural network models with different composite modes for multi-temporal satellite image change detection, and the final experiment proved that the siamese network achieved the best performance (Daudt et al., 2018). In addition, some network architectures focus on feature extraction combined with pre-disaster and post-disaster images. Some methods utilized two regions with CNN feature(R-CNN) models with shared weight to extract the features on pre-disaster and post-disaster images and classify the damage level of buildings after connecting them into one feature (Weber and Kané, 2020). RescueNet (Gupta and Shah, 2021) is a unified model for building segmentation and damage classification tasks. Átrous Spatial Pyramid Pooling (ASPP) module was used on top of the backbone CNN features to obtain multi-scale features in pre-disaster and post-disaster images. Then change detection head utilizes the temporal features to classify each pixel into the damage categories.

3. METHOD

This section introduces the methods of this paper. First, we give an overview of the whole pipeline. The architectures of the xBD baseline model and LEDNet model are introduced. Finally, we computed influence maps to estimate the damage level of power facilities.

3.1 Overview

Our pipeline consists of two stages, as shown in Figure 2. In the first stage, an image segmentation task was performed for a pre-disaster satellite image. Pixels were divided into two categories: building and nonbuilding. Based on the mask of the building, polygons of each building were computed. Furthermore, the bounding boxes of polygons were extracted and used to crop the post-disaster image to obtain the image patches containing the building. More specifically, each image patch contains one building. In the second stage, a damage level classification task was performed to assess the damage scale of each building in the image patch. There are four categories to indicate the level of damage: "no-damage", "minor-damage", "major-damage", "destroyed"(see Table 1). Based on the above results, a group of influence maps was computed for power facilities according to the assessment of buildings damage. We estimated the damage

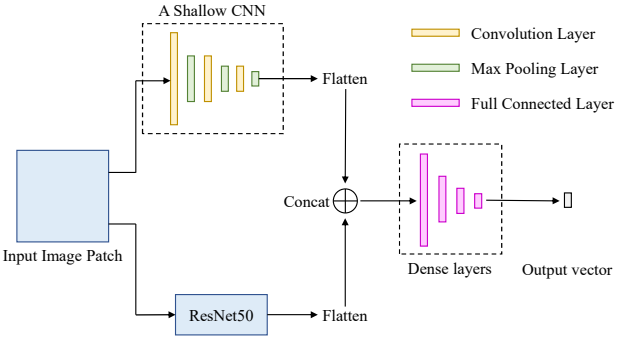

Figure 3. Architecture of network model in the xBD baseline for damage level classification.

level to the electrical facilities based on the building damage assessment results.

3.2 Architecture of the xBD baseline

As mentioned in Section 2.2, two separate networks were used to solve the problems of building segmentation and damage level classification in the xBD baseline. For building segmentation, a pre-disaster satellite image was fed to a modified U-Net (Ronneberger et al., 2015). The damage level classification used a ResNet50 (He et al., 2016) backbone pre-trained on ImageNet (Deng et al., 2009) with ReLU activation in all convolutional layers, as shown in Figure 3. Besides, additional features from shallow convolutional neural networks were concatenated with the output from ResNet50 and passed into dense layers for a one-hot encoded vector output. Each element in the vector represents the probability of ordinal class.

Notably, the damage levels of different buildings are interrelated. For example, the loss between category "no-damage" and category "destroyed" is more significant than category "no-damage" and category "minor-damage". The traditional cross-entropy loss function can not accurately describe this situation, so the xBD baseline utilized the ordinal cross-entropy loss function instead. Unlike traditional methods, ordinal cross-entropy loss considers the distance between the ground truth and the predicted class and gives the network model the ability to distinguish between different levels of damage.

3.3 LEDNet for building segmentation

In this paper, we replaced the U-Net with LEDNet (Wang et al., 2019) for building segmentation. LEDNet employed an asymmetric encoder-decoder architecture for semantic segmentation in real-time, as shown in Figure 4. The encoder included a split shuffle non-bottleneck (SS-nbt) unit and a down-sampling unit. In the SS-nbt unit, two operators, channel split and shuffle, were added in the residual layer to balance performance and efficiency. This unit can be regarded as a feature reuse strategy that expands network capacity but does not significantly increase computational complexity. The downsampling unit can make the deep neural network reduce the amount of computation when extracting information. Inspired by the attention mechanism, the attention pyramid network(APN) was applied to integrate features from three different pyramid scales in the decoder. Depending on the pyramid architecture, APN can capture cues at multiple scales, expand receptive fields, and generate pixel-level attention to features of the convolution layer. The building segmentation stage can execute faster with better accuracy, benefiting from the asymmetric encoder-decoder architecture. More experimental details are in Section 4.4.

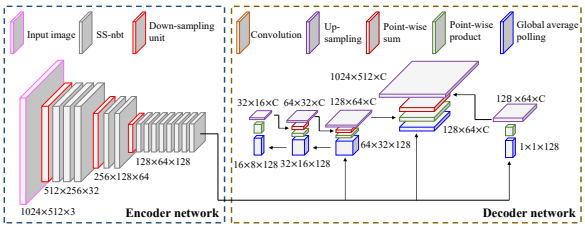

Figure 4. Architecture of LEDNet.

3.4 Damage assessment for electrical facilities

It is equally important to grasp the damage of power facilities in time. However, the xBD dataset (see Section 4.1) has no label of power facilities. Therefore, we compute influence maps to infer the damage of nearby power facilities based on the leverage of affected buildings.

At first, we stratified the damage results of the building according to the damage level. In other words, there were four image layers representing the building mask of four damage levels, "no-damage", "minor-damage", "major-damage" and "destroyed". We call that "hierarchical damage layers", denoted by the symbol $\boldsymbol{L}_i$, where $i = 1, 2, 3, 4$ indicates the ID of damage level in Table 1. Considering that the closer the distance between power facilities and a building, the more similar the damage scale is to the building, we computed the influence maps. We marked the influence map for corresponding hierarchical damage layer $\boldsymbol{L}_i$ as $\boldsymbol{I}_i$. $\boldsymbol{L}_i$ and $\boldsymbol{I}_i$ have the same size.

For the mask of building $\boldsymbol{M}_{i,j}$ in $\boldsymbol{L}_i$,

$$\boldsymbol{I}_{i,j}(\boldsymbol{p}) = W(D(\boldsymbol{p}, \boldsymbol{M}_{i,j})) \tag{1}$$

where $\boldsymbol{I}_{i,j}$ = the influence map for $\boldsymbol{M}_{i,j}$
j = the ID of building mask in $\boldsymbol{L}_i$
$\boldsymbol{p}$ = image coordinate in $\boldsymbol{L}_i$
$\boldsymbol{I}_{i,j}(\boldsymbol{p})$ = the value at position $\boldsymbol{p}$ in $\boldsymbol{I}_{i,j}$
$D(\boldsymbol{p}, \boldsymbol{M}_{i,j})$ = the distance between $\boldsymbol{p}$ and $\boldsymbol{M}_{i,j}$

In the code implementation for $D(\boldsymbol{p}, \boldsymbol{M}_{i,j})$, we use OpenCV to extract the footprint of the building polygon mask $\boldsymbol{M}_{i,j}$ and calculate the distance to $\boldsymbol{p}$. In particular, we set $D = 0$ if $\boldsymbol{p} \in \boldsymbol{M}_{i,j}$.

As the influence of buildings on surrounding pixels decreases rapidly with the increase of distance, we designed function W to weight the distance D in the following way to model this non-linear transformation:

$$W(D) = -\frac{2}{1 + \exp\left(-\alpha\,|D|\right)} + 2 \tag{2}$$

where $W(D)$ = transformed distance D
α = range factors

Notice that $1 \geq W(D) > 0$, and α are range factors that represents the strength of influence of damaged buildings. Especially if there are no building masks in $\boldsymbol{L}_i$, we set $\boldsymbol{I}_i(\boldsymbol{p}) = 0$ for each $\boldsymbol{p}$. Visualized influence maps $\boldsymbol{I}_{i,j}$ are shown in Figure 5.

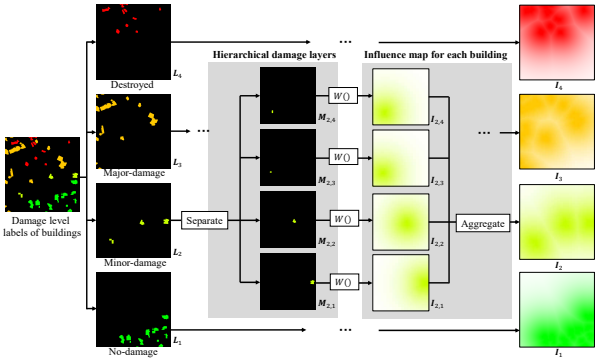

Figure 5. Calculation of influence map.

Table 1. Joint damage scale descriptions in the xBD dataset.

Damage level	ID	Description
Unclassified	0	The damage level could not be determined, usually due to cloud cover or building areas being cropped to the edge of a satellite image.
No-damage	1	No affected, no sign of water, structural or shingle damage.
Minor-damage	2	Water surrounding building, roof elements missing or visible cracks.
Major-damage	3	Partial wall or roof collapse, or surrounded by water and mud.
Destroyed	4	Completely collapsed, partially or entirely covered with water and mud.

For damage level i, influence map $\boldsymbol{I}_i$ was aggregated by the following strategy.

$$\boldsymbol{I}_i\left(\boldsymbol{p}\right) = \max \boldsymbol{I}_{i,j}\left(\boldsymbol{p}\right) \tag{3}$$

Finally, the damage level of electrical facilities can be inferred from each damage level of buildings:

$$l(\boldsymbol{p}) = \sum_i \beta_i \boldsymbol{I}_i(\boldsymbol{p}) + 1 \tag{4}$$

where β_i = damage level weighting factor
$l(\boldsymbol{p})$ = estimated damage level ID (see Table 1)

In general, $l(\boldsymbol{p})$ is not an integer, but we can still refer to Table 1 to get the damage level of power facilities.

Figure 5 shows the framework of this algorithm. For visualization purposes, different damage levels are represented in different colors. The darker the pixel in the influence map, the more significant the impact of nearby buildings on the electrical infrastructure that land on the position of this pixel.

4. EXPERIMENTS

In this section, we introduce the xBD dataset and the metric for evaluation. After that, qualitative and quantitative evaluation about the assessment of buildings and electrical facilities show the effectiveness of our method.

4.1 xBD Dataset

We used the xBD dataset (Gupta et al., 2019) to train and evaluate our network model. xBD dataset is the first building damage assessment dataset, including high-resolution satellite images of 19 natural disaster data of earthquakes, volcanoes, forest fire, flood, typhoon and other types, covering more than 45000 square kilometers of Guatemala, Portugal and the United States. DigitalGlobe provided 1024×1024 satellite images of the same area before and after the disaster within 24 to 48 hours. Each pixel in the image represents 30cm on the ground. The dataset provides over 850,000 building polygons. More specifically, the xBD dataset provides labels for each building polygon in post-disaster images with joint damage scale, including four levels of no-damage, minor-damage, major-damage, and destroyed, as shown in Table 1. In addition, satellite images also contain meta-data, including the capture time, the satellite's attitude relative to the ground, the name of the satellite, the type and location of natural disasters, which can be used for other analyses.

4.2 Training

We were concerned about two types of disasters types, flood, and earthquake. Therefore, images belonging to these two types of disasters in the training set of the xBD dataset were used to train our network model, in which 25% of the images constitute the verification set. In addition, we noticed a large number of images with floods caused by a hurricane, so we also use images that meet these conditions to enrich the training set. LEDNet was trained as a binary semantic segmentation network for building segmentation. In the first stage, the network only focuses on where buildings exist on the pre-disaster satellite images and ignores the damage of buildings in corresponding regions. To classify building damage level, we cropped the post-disaster image in the bounding box of each buildings' polygon from ground truth. These image patches were sent to the ResNet50 backbone network for training.

4.3 Metrics

Similar to the metric proposed in the xBD dataset, we use the F1 score as the accuracy metric for building damage assessment. For each damage level i showed in Table 1.

$$F1_i = \frac{2TP_i}{2TP_i + FP_i + FN_i} \tag{5}$$

where TP_i = the number of true-positive pixels
FP_i = the number of false-positive pixels
FN_i = the number of false-negative pixels
$F1_i$ = the F1 score of damage scale i

The evaluation metric $F1$ for the final damage scale classification is defined as the harmonic mean of the F1 scores for all damage scales:

$$F1 = 4\sum_{i=1}^{4} \frac{1}{F1_i} \tag{6}$$

Note that the category "unclassified" was not considered.

Table 2. Quantitative evaluation for buildings damage assessment.

Methods	Overall ($F1$)	No-damage ($F1_1$)	Minor-damage ($F1_2$)	Major-damage ($F1_3$)	Destroyed ($F1_4$)
U-Net + ResNet50 (xBD baseline)	0.3661	0.7954	**0.0968**	0.0922	0.4799
LEDNet + ResNet50 (ours)	**0.3739**	**0.8080**	0.0943	**0.1084**	**0.4851**

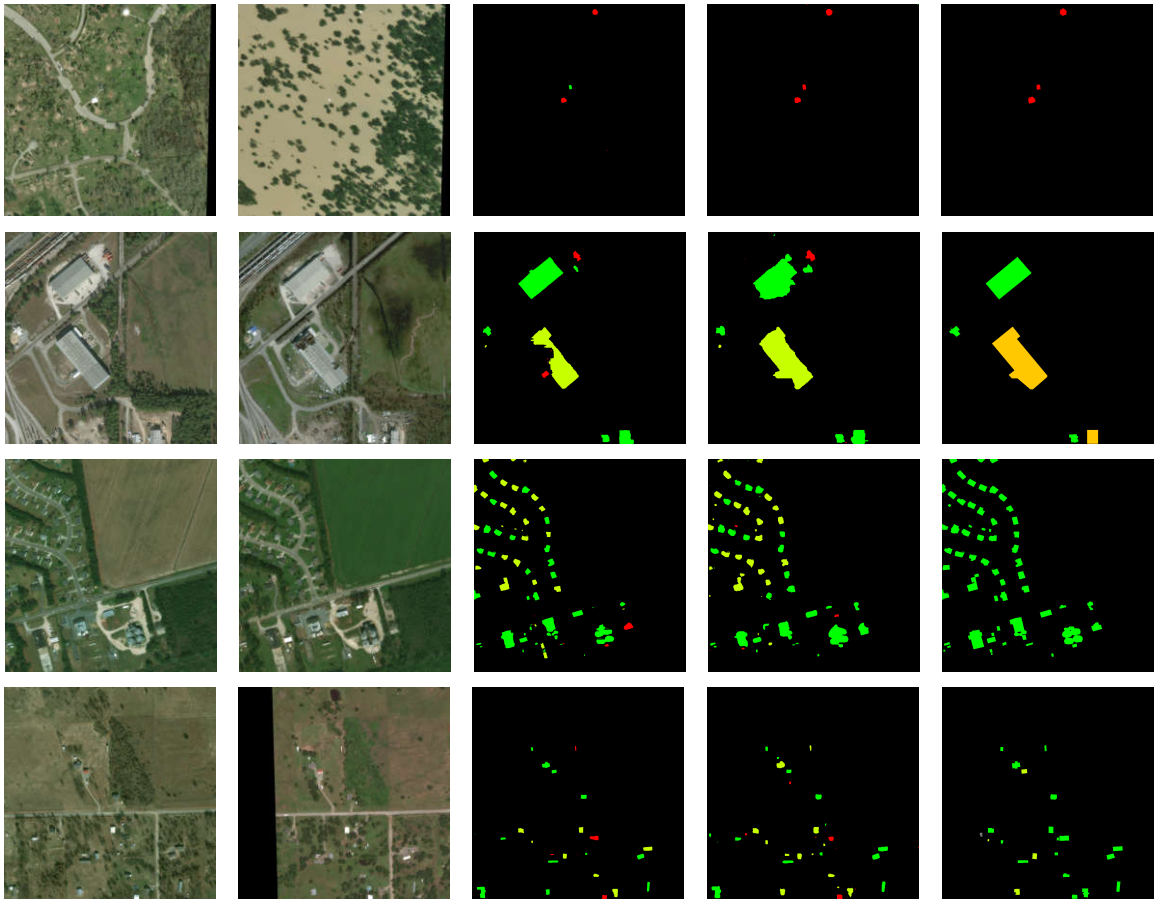

Figure 6. Qualitative evaluation for building damage assessment.

4.4 Evaluation of building damage assessment

In order to evaluate our method, we utilized the images in the xBD dataset testing set for evaluating performance. Similarly, we only used images of disasters such as floods and earthquakes, and those images with floods caused by hurricanes were also used for evaluation.

Table 2 shows the quantitative evaluation results of the xBD baseline and our methods for building damage assessment. Compared with the xBD baseline, our method is more accurate in most damage levels. In terms of time consumption, the improvement of our method is in the segmentation stage. For LEDNet, the average time on the images in the testing set was 23.62ms, while U-Net was 147.38ms. Our method is about six times faster than the xBD baseline for building segmentation.

Figure 6 shows the qualitative evaluation results. The first and second columns represent the pre-disaster and post-disaster satellite images. The third and fourth columns are the building damage assessment results of the xBD baseline and our method. The same as Figure 1 (c) and Figure 1 (d), different colors of pixels represent different damage levels: green is “no-damage”, yellow-green is “minor-damage”, orange is “major-damage”, and red is “destroyed”. The black pixels in the background mean there are no buildings. The last column in Figure 6 is the ground truth. In particular, the damage level of some buildings in the ground truth is “unclassified”, which is indicated in gray in the Figure. We selected some representative images of floods and earthquakes in US and Mexico. In the first row, the results of our method have higher precision for the small building mask near the image center. In the second row, we see that the buildings in the image center segmented by our method are complete, whereas the mask segmented by the xBD baseline is fragmentary.

Compared with the xBD baseline, the building masks segmented by LEDNet are more expansive, as shown in the third row of Figure 6. This advantage allows the image patches to retain more information around the building, conducive to more accurate damage classification by ResNet50. That is why the proposed method’s accuracy is higher than the xBD baseline. However, constrained by the lightweight architecture of the network, LEDNet has difficulties in processing high-resolution satellite

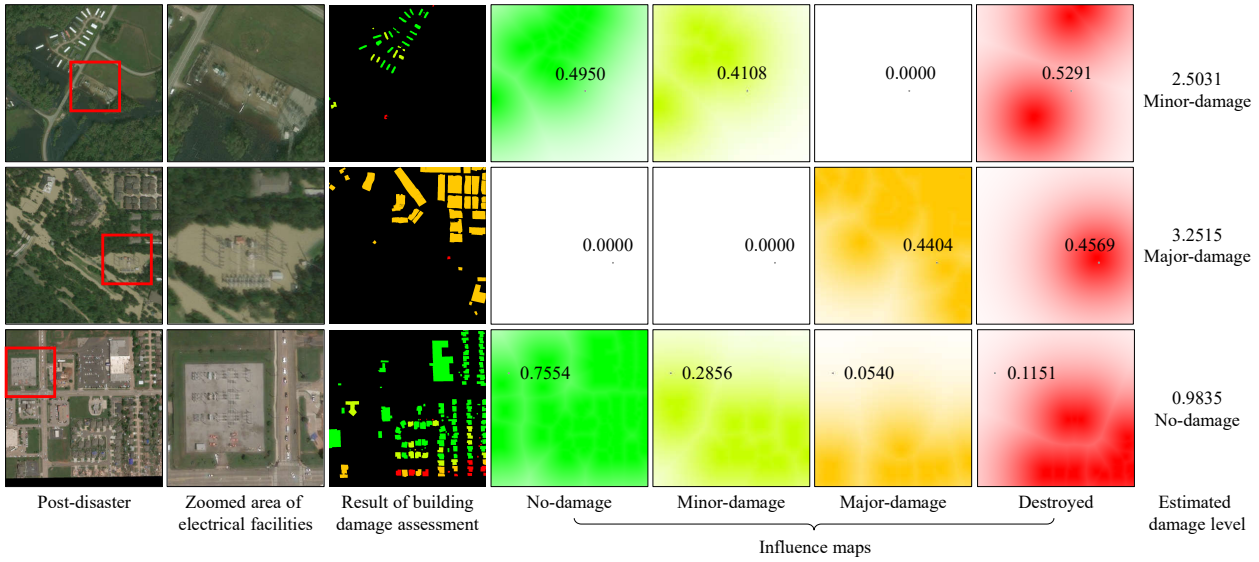

Figure 7. Qualitative evaluation for electrical facilities damage assessment.

images. It only improves the accuracy of our method a little bit. Besides, we find both xBD baseline and our methods unable to handle cloud-covered and cropped satellite images. For instance, the left side of the post-disaster image in the last row of Figure 6 is cropped out, while the corresponding pre-disaster image is unbroken. xBD baseline and our methods only segment the pre-disaster image so that the image patches of fake buildings on the left-bottom corner were classified, while the ground truth has no buildings in the same area. This defect reduces the final accuracy.

4.5 Evaluation of electrical power facilities assessment

This section introduces qualitative evaluation for electrical facility damage assessment. As shown in Figure 7, we calculate the influence maps based on the building damage level information. The first column is the post-disaster image, and the high-light area by the red box is zoomed in the second column, which shows more details of the electrical utilities. The damage to the building is shown in the third column. The following four columns are influence maps for each damage level. Influence maps with different damage levels were colored with different colors for visualization. Darker pixels indicate more powerful influence from nearby buildings and vice versa. Besides the points sits the center of electrical facilities. We can get the estimated damage level of electrical by equation 4 in the last column in Figure 7.

In our experiment, $\alpha = 0.005$, $\beta_0 = 0$, $\beta_1 = -1$, $\beta_2 = 1$, $\beta_3 = 2$, $\beta_4 = 3$. From the first row in Figure 7, our method inferred that the damage level of this power facility is "minor-damage". The fact is consistent with the above result that some power facilities have been flooded. Similarly, the substation in the second row was completely flooded, and the estimated damage level "major-damage" is consistent with the reality. In the third row, most buildings at the bottom of the image were destroyed. By referring to buildings closer to the electric facilities, our algorithm can still get reasonable results of "no-damage". That is consistent with the fact that we cannot find any damage to the electrical infrastructure from the satellite imagery.

Our approach is based on common sense that damage to electrical facilities and surrounding buildings is usually the same. However, if the number of buildings around power facilities is insufficient, it is difficult to obtain accurate damage estimation by our method. This problem will be solved in further study.

5. CONCLUSIONS

This paper describe a dual-stage pipeline that uses pre-disaster and post-disaster satellite images to assess building damage. We replaced U-Net in the xBD baseline for the lightweight network LEDNet, which improves accuracy and inference speed. Considering that power facilities are equally crucial for disaster relief, we computed influence maps to assess the damage level for electrical facilities by combining the damage scale of the building. Evaluations on the xBD dataset demonstrated the effectiveness of the proposed method.

We believe that using a unified network architecture to solve this problem is the most effective. It can make building segmentation and damage assessment use common features, conducive to simultaneously improving accuracy and processing speed. In order to gather more details for more accurate damage assessment, expanding the receptive field is also helpful for the analysis of high-resolution satellite images. This is the direction of our future study.

ACKNOWLEDGEMENTS

The author's work are supported by the project (No.YNKJXM20191246) on the research and application of constructing satellite remote sensing technology power application comprehensive test site and environment wide area intelligent monitoring.

REFERENCES

Badrinarayanan, V., Kendall, A., Cipolla, R., 2017. Segnet: A deep convolutional encoder-decoder architecture for image segmentation. *IEEE transactions on pattern analysis and machine intelligence*, 39(12), 2481–2495.

Bochkovskiy, A., Wang, C.-Y., Liao, H.-Y. M., 2020. Yolov4: Optimal speed and accuracy of object detection. *arXiv preprint arXiv:2004.10934*.

Cai, H., Meng, F., Yang, S., Guo, R., Wang, X., Xiang, L., 2021. Modeling and analyzing of waterlogging in typical urban area. *2021 7th International Conference on Hydraulic and Civil Engineering Smart Water Conservancy and Intelligent Disaster Reduction Forum (ICHCE SWIDR)*, 37–42.

Chen, T., 2021. Interpretability in Convolutional Neural Networks for Building Damage Classification in Satellite Imagery.

Cooner, A. J., Shao, Y., Campbell, J. B., 2016. Detection of urban damage using remote sensing and machine learning algorithms: Revisiting the 2010 Haiti earthquake. *Remote Sensing*, 8(10), 868.

Daudt, R. C., Le Saux, B., Boulch, A., 2018. Fully convolutional siamese networks for change detection. *2018 25th IEEE International Conference on Image Processing (ICIP)*, IEEE, 4063–4067.

Deng, J., Dong, W., Socher, R., Li, L.-J., Li, K., Fei-Fei, L., 2009. Imagenet: A large-scale hierarchical image database. *2009 IEEE conference on computer vision and pattern recognition*, Ieee, 248–255.

Doshi, J., Garcia, D., Massey, C., Llueca, P., Borensztein, N., Baird, M., Cook, M., Raj, D., 2019. Firenet: Real-time segmentation of fire perimeter from aerial video. *arXiv preprint arXiv:1910.06407*.

Fujita, A., Sakurada, K., Imaizumi, T., Ito, R., Hikosaka, S., Nakamura, R., 2017. Damage detection from aerial images via convolutional neural networks. *2017 Fifteenth IAPR international conference on machine vision applications (MVA)*, IEEE, 5–8.

Gupta, R., Hosfelt, R., Sajeev, S., Patel, N., Goodman, B., Doshi, J., Heim, E., Choset, H., Gaston, M., 2019. xbd: A dataset for assessing building damage from satellite imagery. *arXiv preprint arXiv:1911.09296*.

Gupta, R., Shah, M., 2021. Rescuenet: Joint building segmentation and damage assessment from satellite imagery. *2020 25th International Conference on Pattern Recognition (ICPR)*, IEEE, 4405–4411.

Hao, H., Baireddy, S., Bartusiak, E. R., Konz, L., LaTourette, K., Gribbons, M., Chan, M., Comer, M. L., Delp, E. J., 2020. An attention-based system for damage assessment using satellite imagery. *arXiv preprint arXiv:2004.06643*.

He, K., Gkioxari, G., Dollár, P., Girshick, R., 2017. Mask r-cnn. *Proceedings of the IEEE international conference on computer vision*, 2961–2969.

He, K., Zhang, X., Ren, S., Sun, J., 2016. Deep residual learning for image recognition. *Proceedings of the IEEE conference on computer vision and pattern recognition*, 770–778.

Ji, M., Liu, L., Buchroithner, M., 2018. Identifying collapsed buildings using post-earthquake satellite imagery and convolutional neural networks: A case study of the 2010 Haiti earthquake. *Remote Sensing*, 10(11), 1689.

Liu, H., Wang, Z., Shang, F., Zhang, M., Gong, M., Ge, F., Jiao, L., 2019. A novel deep framework for change detection of multi-source heterogeneous images. *2019 International Conference on Data Mining Workshops (ICDMW)*, IEEE, 165–171.

Lyu, H., Lu, H., Mou, L., 2016. Learning a transferable change rule from a recurrent neural network for land cover change detection. *Remote Sensing*, 8(6), 506.

Margesson, R., Taft-Morales, M., 2010. Haiti earthquake: Crisis and response. Library of Congress Washington DC Congressional Research Service.

Nex, F., Duarte, D., Tonolo, F. G., Kerle, N., 2019. Structural building damage detection with deep learning: Assessment of a state-of-the-art cnn in operational conditions. *Remote sensing*, 11(23), 2765.

Papadomanolaki, M., Verma, S., Vakalopoulou, M., Gupta, S., Karantzalos, K., 2019. Detecting urban changes with recurrent neural networks from multitemporal sentinel-2 data. *IGARSS 2019-2019 IEEE International Geoscience and Remote Sensing Symposium*, IEEE, 214–217.

Qi, Z., Yeh, A. G.-O., Li, X., Zhang, X., 2015. A three-component method for timely detection of land cover changes using polarimetric SAR images. *ISPRS Journal of Photogrammetry and Remote Sensing*, 107, 3–21.

Rahnemoonfar, M., Chowdhury, T., Sarkar, A., Varshney, D., Yari, M., Murphy, R., 2020. Floodnet: A high resolution aerial imagery dataset for post flood scene understanding. *arXiv preprint arXiv:2012.02951*.

Ronneberger, O., Fischer, P., Brox, T., 2015. U-net: Convolutional networks for biomedical image segmentation. *International Conference on Medical image computing and computer-assisted intervention*, Springer, 234–241.

Van Etten, A., 2018. You only look twice: Rapid multi-scale object detection in satellite imagery. *arXiv preprint arXiv:1805.09512*.

Wang, Y., Zhou, Q., Liu, J., Xiong, J., Gao, G., Wu, X., Latecki, L. J., 2019. Lednet: A lightweight encoder-decoder network for real-time semantic segmentation. *2019 IEEE International Conference on Image Processing (ICIP)*, IEEE, 1860–1864.

Weber, E., Kané, H., 2020. Building disaster damage assessment in satellite imagery with multi-temporal fusion. *arXiv preprint arXiv:2004.05525*.

Wen, F., Adhikari, L., Pei, L., Marcia, R. F., Liu, P., Qiu, R. C., 2017. Nonconvex regularization-based sparse recovery and demixing with application to color image inpainting. *IEEE Access*, 5, 11513–11527.

Xiong, S., Liu, Y., Yan, Y., Pei, L., Xu, P., Fu, X., Jiang, X., 2021. Object recognition for power equipment via human-level concept learning. *IET Generation, Transmission & Distribution*, 15(10), 1578–1587.

Xu, J. Z., Lu, W., Li, Z., Khaitan, P., Zaytseva, V., 2019. Building damage detection in satellite imagery using convolutional neural networks. *arXiv preprint arXiv:1910.06444*.

Zhang, L., Xia, J., 2022. Flood Detection Using Multiple Chinese Satellite Datasets during 2020 China Summer Floods. *Remote Sensing*, 14(1), 51.